A Laser-Induced Traveling-Wave Device for Generating Millimeter Waves

JACK SOOHOO, SHI-KAY YAO, SENIOR MEMBER, IEEE, JAMES E. MILLER, RICHARD R. SHURTZ, II, YUAN TAUR, AND R. A. GUDMUNDSEN, SENIOR MEMBER, IEEE

Abstract—**We have investigated a novel device concept for generating CW millimeter waves with output power in the multiwatt range. The concept involves the utilization of modulated laser radiation to induce in a distributed Schottky-diode structure a traveling-wave current which, in turn, synchronously excites the dominant mode of a waveguide structure to generate millimeter power. The induced traveling-wave current is directly proportional to the laser modulation generated by the interference of two overlapping laser beams of millimeter beat frequency. Detailed analysis indicates that the device has both high-output and frequency-tunable characteristics.**

THE RAPID technological development of solid-state millimeter-wave components over the past few years has renewed significant interest in the exploitation of that portion of the electromagnetic spectrum. As for the state-of-the-art CW millimeter-wave sources, existing gyrotron and tube-type systems are capable of generating very high output power (in the kilowatt range), but these systems are large in size and weight and, therefore, impractical for most applications. Compact solid-state transit-time devices such as IMPATT diodes can produce about a watt of CW power at 100 GHz, but their output power drops rapidly with increasing frequency, to only tens of milliwatts near 200 GHz. Although various power-combine techniques (at both device and circuit levels) have been used to coherently combine the output of individual IMPATT diodes, these techniques have not been satisfactory, mainly due to the rapid increase of insertion and path losses as the number of diodes increases. At present, a compact solid-state millimeter source capable of generating even a few watts of CW power is still unavailable.

This paper is concerned with a traveling-wave solid-state device for generating CW millimeter waves with output power in the multiwatt range. The concept is simply illustrated in Fig. 1. It involves the excitation of a waveguide structure with a traveling-wave current to produce millimeter waves under phase-matching condition, very similar to the concept of a phased-array antenna. Here, the current source is a consequence of the laser-induced carriers within the depletion layer of a reverse-biased strip Schottky diode

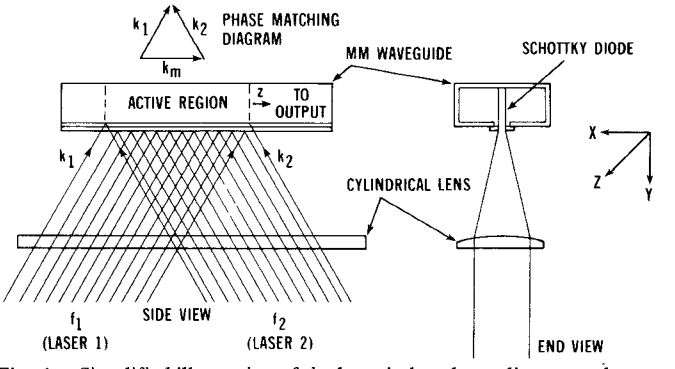

Fig. 1. Simplified illustration of the laser-induced traveling-wave device.

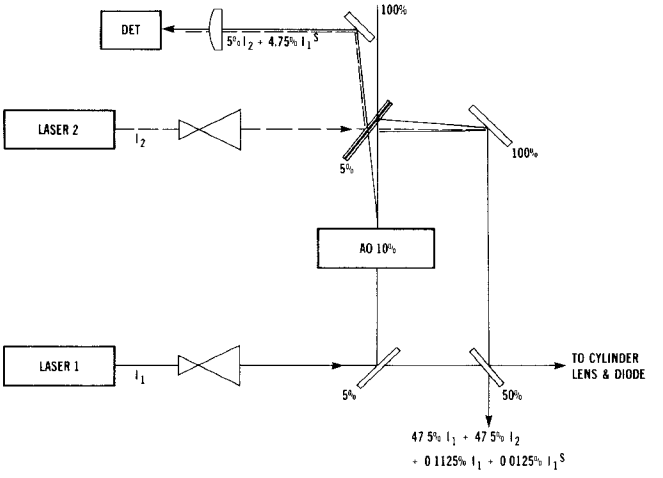

Fig. 2. Functional block diagram of the traveling-wave device.

which, itself, is part of the millimeter-wave structure. The diode is reverse biased to saturation so that the carriers are swept out of the depletion layer at their saturation velocity. These carriers are generated through the absorption of energy from the two interfering laser beams of millimeter beat frequency. Fig. 2 is a functional block diagram of the device. The laser intensities, I_1 and I_2, are approximately equal. With the RF frequency of the AO cell as reference, the detector output drives a feedback loop (not shown) which, in turn, controls and stabilizes the laser beat frequency, or the output millimeter frequency. The angle between the two laser beams, which determines the phase velocity of the excited millimeter energy, is controlled by the turn mirror. The device is potentially compact and lightweight, because the required laser energy for excitation may be provided by small sealed-off waveguide lasers.

Manuscript received March 25, 1981; revised July 13, 1981.

J. SooHoo and R. A. Gudmundsen are with Rockwell International, Anaheim, CA 92803.

S. K. Yao is with TRW, Torrance, CA 90509.

J. E Miller and R. R. Shurtz, II, are with Night Vision and Electo-Optics Laboratory, Fort Belvoir, VA 22060.

Y. Taur is with Rockwell International, Thousand Oaks, CA 91360.

0018-9480/81/1100-1174$00.75 ©1981 IEEE

II. General Considerations

A. Laser Power and Induced Current

The traveling-wave current in the depletion layer is induced by two overlapping laser beams. As depicted in Fig. 1 , the total electric field of the two lasers, E, in the depletion layer may be expressed as

$$E=E_0\exp i\left(\omega_1 t+k_1 z\sin\frac{\theta}{2}\right)+E_0\exp i\left(\omega_2 t-k_2 z\sin\frac{\theta}{2}\right) \tag{1}$$

where z is the direction along the waveguide axis, θ is the angle between the two beams of equal amplitude E_0, ω_i and k_i, $i=1$ or 2, are the laser frequencies and propagation constants, respectively. The effective laser intensity I illuminating the depletion layer is then of the form

$$I\sim|E|^2=2E_0^2\left\{1+\cos\left[(\omega_2-\omega_1)t-(k_2+k_1)z\sin\frac{\theta}{2}\right]\right\} \tag{2}$$

which is a traveling wave oscillating at the beat frequency $\omega_2-\omega_1$. Thus the induced current is also a traveling wave since it is directly proportional to the laser intensity. While the dc term of the induced current contributes to heat generation, the ac term is a current source of frequency ω and of phase velocity V_p given by

$$\omega=\omega_2-\omega_1$$
$$V_p=\frac{\omega_2-\omega_1}{(k_2+k_1)\sin\frac{\theta}{2}}. \tag{3}$$

B. Material Absorptivity and Transit Time

To determine the effect of the material absorptivity, α, we consider a strip Schottky-diode structure consisting of an n-type layer sandwiched between a metal layer (M) and an n^+-layer substrate. In this M-n-n^+-configuration, the absorptivity of the n^+-substrate at the laser wavelength is made negligible compared with that of the active n-layer of thickness W. Let Φ be the incident photon flux entering the depletion region at $x=0$. Then the induced current density J in amperes per unit area is [1]

$$J=-q\Phi(1-e^{-\alpha W}) \tag{4}$$

where q is the magnitude of the electron charge.

Assuming saturated drift velocity V_s, the maximum density of electron–hole pairs n, generated by an optical flux density Φ, is given by

$$n=\frac{J}{qV_s}=\frac{\phi(1-e^{-\alpha W})}{V_s}. \tag{5}$$

Assuming an input power of 2 W at a wavelength of 5.5 μm, the maximum electron–hole density is 1.05×10^{14} cm^{-3} in the depletion layer. The space charge field generated by this plasma is given by [2]

$$E=\frac{JW}{V_s\epsilon}=\frac{qnW}{\epsilon} \tag{6}$$

where ϵ is the dielectric constant. For the photogenerated pair density calculated above, a depletion-layer width of 1 μm, and the material parameters given in Table III, the space charge field is calculated to be 1.1×10^3 V/cm, which is well below the applied field ($\sim2\times10^4$ V/cm). Therefore, quasi-charge neutrality conditions leading to an ambipolar type of diffusion process are not relevant. Drift, not diffusion, dominates carrier flow through the depletion layer.

As the laser flux traverses the depletion layer, the contribution to the total current from individual electrons generated at a given point x along the path has a relative phase factor $e^{-i\omega(W-x)/V_s}$. For the worst case, in which we assume the electrons are uniformly generated within the entire depletion layer, the transit-time degradation factor B is simply obtained by averaging the phase factor as follows:

$$B=\frac{\int_0^W e^{-(\omega/V_s)dx}}{W}=\frac{\sin\omega\tau/2}{\omega\tau/2} \tag{7}$$

where $\tau=W/V_s$, the transit time across the depletion layer. Thus the induced millimeter-wave current density taking into account the effect of both transit time and absorptivity is of the form

$$J=J_0(1-e^{-\alpha W})\frac{\sin\omega\tau/2}{\omega\tau/2}\cos\omega(t-z/V_p) \tag{8}$$

where J_0 is in amperes per unit area.

C. Laser and Material Parameters

Since a single photon can generate at most one electron–hole pair, long-wavelength lasers (e.g., CO and CO_2) are more efficient and, therefore, narrow-gap infrared materials are of particular interest for this application. Two partial lists of CO lasing lines which would yield millimeter frequencies are given in Tables I and II.

Equation (8) indicates that the values of absorptivity, saturation velocity, and responsivity should be large for

TABLE I
PARTIAL LIST OF CO LASER TRANSITIONS WITH BEAT FREQUENCIES NEAR 240 GHz

Transition	λ(um)	ν(cm^{-1})	Beat Frequency (GHz)	λ(mm)
P(13)	5.45	1833.51		
P(14)	5.47	1829.59	237.0	1.266
P(15)	5.48	1825.61	239.7	1.252
P(16)	5.49	1821.60	241.5	1.242
P(17)	5.50	1817.56	243.0	1.235
P(18)	5.51	1813.50		

TABLE II
PARTIAL LIST OF CO LASER TRANSITIONS WITH BEAT FREQUENCIES NEAR 95 GHz

	Transitions	Beat Frequency	λ(mm)	λ(um)
1.	11-10 P(11) and 9-8 P(24)	94.8 GHz	3.165	5.43
2.	10-9 P(23) and 9-8 P(28)	93.9 GHz	3.195	5.50
3.	9-8 P(12) and 8-7 P(19)	95.7 GHz	3.135	5.30

TABLE III
PARAMETER VALUES OF HgCdTe AT 77 K

Parameters	Values
Absorptivity (α)	$\gtrsim 10^5$ m^{-1}
Saturation Velocity (v_s)	4×10^5 M/S
Dielectric Constant (ϵ/ϵ_0)	17
Thermal Conductivity (K)	0.2 Watt/C°/cm
Breakdown Voltage (V_b)	Greater than 2 Volt

efficient current generation. A material with a large thermal conductivity would minimize the thermal problem through rapid heat conduction, which is especially important for high-power generation. In order to minimize the adverse effects of the diode capacitance and series resistance, which limit the frequency response and contribute to RF loss, the dielectric constant of the material should not be overly large but the n^+-layer doping be high. The depletion-layer width which is limited because of the transit-time effect must also approximately satisfy the equation

$$W \simeq \sqrt{\frac{2\epsilon V_b}{qN_d}} \tag{9}$$

where V_b is the bias voltage, N_d is the doping concentration of the n layer, and ϵ is the dielectric constant. The narrow-gap mixed crystal HgCdTe appears to be a good candidate material to be used with the CO lasers operating at around 5-μm wavelength and will be used for the configuration design. The parameter values of this material are given in Table III.

III. Formulation of Traveling-Wave Source Concept

A simple transmission-line model may be used to understand the traveling-wave process. For the optically induced current distribution under consideration, however, waveguide configurations are more efficient for power generation because of their inherently strong source-to-field coupling characteristics. We will first develop the transmission-line approach to gain some physical insights, and then develop the waveguide model.

A. Transmission-Line Model

It is easy to show from the transmission-line equations that the transverse voltage V of a transmission line driven by a traveling-wave current source with the direction of propagation along z satisfies

$$\frac{d^2V}{dz^2} - ZYV = -ZJ'e^{-i\beta' z}, \qquad z_1 \leqslant z \leqslant z_2 \tag{10}$$

where $z_1 < z < z_2$ is the source region, Z is the series impedance per unit length of the line, Y is the shunt admittance per unit length of the line, J' is the current amplitude, and β' is the propagation constant of the current source. For convenience, we have omitted the time factor $e^{i\omega t}$ from (10).

The solution of (10) is given by (A16) of Appendix I. The first equation of (A16) describes the voltage propagation to the left from $z=z_1$ to the matching impedance at $z=0$. Since γ is of the form $\gamma=\alpha_c+i\beta$, where α_c is the loss constant and β is the propagation constant of the line itself, the left-going voltage is negligible when the interaction is phase-matched (i.e., $\beta=\beta'$). In contrast, the right-going voltage, as described by the third equation, is "resonantly" large for $\beta=\beta'$. Within the source region, the voltage is described by the second equation of (A16). It has the characteristics of a growing space-transient wave, as expected, because energy is coherently added to the wave in this region.

B. Waveguide Model

The complex electric field $\boldsymbol{E}$ inside a uniform metallic waveguide which is excited by a current per unit area, $\boldsymbol{J}$, with time variation $e^{i\omega t}$ satisfies

$$\nabla^2 \boldsymbol{E} + k^2 \boldsymbol{E} = i\omega\mu \boldsymbol{J} \tag{11}$$

where boldface denotes vector quantities, $k=\omega^2\mu\epsilon$, and μ the permeability. $\boldsymbol{E}$ may be expanded in terms of the waveguide eigenmodes ϕ_{mn} as follows:

$$\boldsymbol{E}(x, y, z) = \sum_{m,n} \boldsymbol{A}_{mn}(z)\phi_{mn}(x, y) \tag{12}$$

where $\boldsymbol{A}_{mn}(z)$ is the z-dependent "amplitude" function. Substituting (12) into (11), multiplying by ϕ_{mn}, and integrating over the waveguide cross section, we obtain

$$\frac{d^2\boldsymbol{A}_{mn}}{dz^2} + \left(k^2 - k_{mn}^2\right)\boldsymbol{A}_{mn} = i\omega\mu \int\int \boldsymbol{J}\phi_{mn}\, dx\, dy \tag{13}$$

k_{mn} being the eigenvalue (i.e., cutoff wavenumber) corresponding to ϕ_{mn}. For $\boldsymbol{J}=J\hat{y}$, (11) simplifies to

$$\frac{d^2A_{mn}}{dz^2} + \left(k^2 - k_{mn}^2\right)A_{mn} = i\omega\mu \int\int J\phi_{mn}\, dx\, dy. \tag{14}$$

We see that the excited mode amplitude A_{mn} is large when the overlap integral is large (i.e., strong source to field coupling). It is usually the dominant or lowest order mode which is excited. In any case, the higher order modes have much larger loss constants and decay rapidly down the guide. We, therefore, assume only the dominant mode is excited and reduce (14) and (12) to

$$\frac{d^2A}{dz^2} + \left(k^2 - k_c^2\right)A = i\omega\mu \int_{-s/2}^{s/2} J\phi(x)\, dx \tag{15}$$

$$E(x, z) = A(z)\phi(x) \tag{16}$$

where $A(z)$ is the dominant mode amplitude, ϕ is the corresponding eigenfunction, and k_c is the cutoff wavenumber.

In deriving (15) and (16), the following assumptions have been made: J is uniform in the transverse directions; the waveguide cross section is symmetrical about $x=0$ with J confined within $-s/2 \leqslant x \leqslant s/2$; and the dominant mode function is y independent. As we shall see, these assumptions are valid and appropriate for the present case.

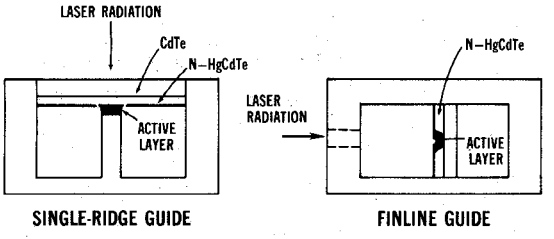

Fig. 3. Cross-sectional views of two low-impedance and wide-band waveguide configurations (not to scale).

IV. Waveguide Design and Numerical Results

A. Possible Configurations

Ideally, the waveguide structure coupled to the source should be wide band, low loss, and should have a low characteristic impedance. A large bandwidth allows frequency tunability and single-mode operation, while low loss allows a longer structure be used, which would minimize the thermal problems and thus increase power-handling capability. A low-impedance configuration is desirable for high-power generation since the diode is voltage limited. Here the characteristic impedance Z_v is defined as

$$Z_v = \frac{V_0^2}{2P} \tag{17}$$

where P is the average power and V_0 is the maximum voltage across the guide. Additionally, the shape and dimensions of the waveguide cross section should be such as to provide strong coupling between the mode fields of the waveguide and the distributed diode current source, as suggested by the overlap integral of (15). Because of the transit-time effect, however, the active HgCdTe layer thickness is necessarily limited to no more than about 2 μm. To minimize the effect of leakage current and to simplify fabrication, the width of the strip diode is probably limited to no more than about 25 μm. The cross-sectional area of the active layer is, therefore, about 2 μm$\times$25 μm, which is small compared to that of a standard rectangular waveguide operating in the millimeter region (i.e., 100 to 300 GHz). This suggests that a ridged rectangular guide be used, with the Schottky-diode modulator filling the gap above the ridge. Such a configuration would provide strong source-to-field coupling, because its dominant mode fields are known to be concentrated in the gap region. Moreover, ridge-guide structures are inherently wide-band and tunable over a wide-frequency range. Although these guides are more lossy than the corresponding rectangular guides, their impedances are much lower and have, therefore, proportionately higher output capability.

Both the single-ridge guide and the fin-line guide, sketched in Fig. 3, would provide strong coupling between the source and the fields, the latter corresponding to a double-ridge guide of negligible ridge thickness. For the single-ridge configuration, confinement of the millimeter energy to the gap is a key (but manageable) concern because of possible millimeter-wave energy loss through the slot above the ridge. The CdTe substrate is a transparent dielectric at the 5-μm laser wavelength, thus absorption of the laser energy, and hence carrier generation, occurs only within the HgCdTe layer. The configuration as illustrated in Fig. 4 would be a good approximation of the ideal single-ridge design, which would not be very difficult to realize. For the fin-line configuration, the HgCdTe layer should not be doped as a conductor, so that it would behave as a dielectric and would not significantly alter the modal fields. Since the fields of these configurations are primarily concentrated in the gap region, guide walls sufficiently away from the gap may be altered for diode biasing without affecting the device performance. Various proven techniques for biasing diodes mounted in this type of structure have been reported in the literature and will not be discussed here [3]. Both the cutoff frequency and the characteristic impedance of these ridge-guide structures are fairly well understood and can be readily calculated [4], [5]. Using these calculations for the ridge-guide configuration neglects the guiding effects of the dielectric within the gap and thus underestimates the field-current coupling efficiency. As might be expected from the "gap" volume consideration, the single-ridge guide has a lower impedance than the fin-line guide and, therefore, the former is superior for high-power generation.

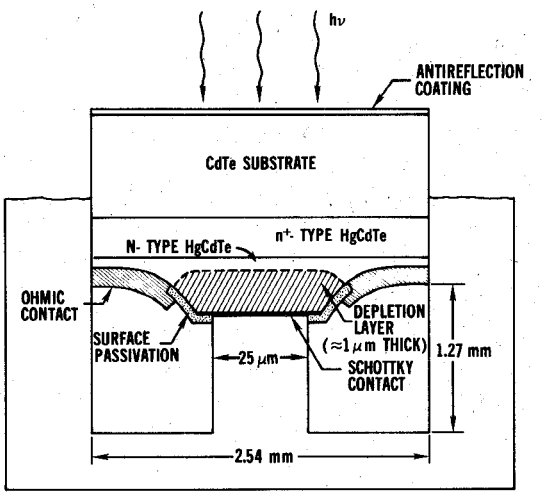

Fig. 4. Single-ridge configuration (not to scale).

B. Device Performance

In this section, analysis and performance calculations are made for a single-ridge configuration having an n-type HgCdTe layer as the active medium. The dominant mode eigenfunction $\phi(x)$ is given by [5]

$$\phi = \begin{cases} \cos(k_c x), & -\frac{a}{2} \leq x \leq \frac{a}{2} \quad \text{and} \quad -d \leq y \leq 0 \\ 0, & \text{elsewhere.} \end{cases} \tag{18}$$

Substituting (18) and the expression for the traveling-wave current into (15), we have

$$\frac{d^2V_0}{dz^2} - \gamma^2 V_0 = i\omega\mu \frac{I_0 e^{-i\beta' z}}{ls} d \frac{2\,\mathrm{sinc}(k_c S/2)}{1+\mathrm{sinc}(k_c S)} \tag{19}$$

TABLE IV
PARTIAL LIST OF PARAMETER VALUES USED IN THE CALCULATIONS

f(GHz)	λ_c(M)	β(M^{-1})	k_c(M^{-1})	α_c(M^{-1})	Z_v(OHMS)	axb(mmxmm)	Standard Waveguide Designation
200	0.016	1.7×10^4	383	39	2.72	1.295x0.6475	WR5
150	0.021	1.3×10^4	298	27	2.69	1.650x0.8255	WR6
100	0.033	8.6×10^3	192	14	2.65	2.540x1.2700	WR10

where $V_0 = Ad$, the maximum voltage across the guide, I_0 is the laser-induced millimeter-current amplitude in the strip diode, $\operatorname{sinc} x = \sin x/x$, $-\gamma^2 \equiv k^2 - k_c^2 = (\alpha_c + i\beta)^2$, and l is the active layer length extending from $z=0$ to $z=l$ along the guide axis. The output power of the device, P, is

$$P = \frac{V_0^2(z=l)}{2Z_v}. \tag{20}$$

V_0 as a function of z in he active region $0 \leqslant z \leqslant l$ is found from the Green's function technique of Appendix II to be

$$V_0 = \frac{Z_0 dI_0}{lS}\left[\frac{\operatorname{sinc}(k_c S/2)}{1+\operatorname{sinc}(k_c S)}\right]\left[\frac{e^{-i\beta z}}{i\delta\beta - \alpha_c}\left(e^{-i\delta\beta z} - e^{-\alpha_c z}\right) + \frac{e^{i\beta z}}{i2\beta}\left(e^{-i2\beta l - i\delta\beta l - \alpha_c(l-z)} - e^{-i2\beta z - i\delta\beta z}\right)\right] \tag{21}$$

where we have substituted $\beta+\delta\beta$ for β' and $z_1=0$ and $z_2=l$. For the ideal phase-matched case, where the current source and the mode fields are in perfect synchronism, $\delta\beta=0$). We have also made the usual assumption that α_c, $\delta\beta \ll \beta$ which is valid for most cases of practical interest. Wave-vector mismatching, $\delta\beta$, may result from misalignment between the lasers or with respect to the waveguide axis. The effect of misalignment on the wave vector is quantitatively studied in Appendix III.

The millimeter power at points along the active region for frequencies 100, 150, and 200 GHz is shown in Figs. 5 and 6. The active length, height, and width of the strip diode used in the calculation are, respective, $l=5$ mm, $S=25$ μm, and $d=1$ μm. These values were chosen from a tradeoff study, taking into account the effect of both transit time and heat generation, as well as the state-of-the-art HgCdTe technology. The induced millimeter current amplitude I_0 in the active region is 2 A, which corresponds to about 1 W of optical power from each of the two CO lasers. For each frequency, the values of λ_c, β, k_c, α_c, and Z_v corresponding to the waveguide a and b dimensions were calculated from [4]–[6]. These and other parameter values are given in Table IV.

In order for the device to have gain, the applied dc voltage must exceed the ac voltage generated by the propagating millimeter wave. DC voltages for three selected power levels are also shown in Figs. 5 and 6. For example, if 2 W of output power is required, the diodes must be reverse biased to at least 4 V.

Fig. 5 shows the effect of the phase-mismatch error due to laser misalignment as discussed in Appendix III. The output power of the device, which is the value of P at $z=l$, is relatively insensitive to the orientation angles ϕ_1 and ϕ_2 for angle values smaller than about 10°. However, the output power is sensitive to the error in θ, especially at higher frequencies. The 10-percent error in θ used in the calculation is probably large, for the nominal values of θ are on the order of milliradians and, therefore, much smaller error should be achievable experimentally. Fig. 6 shows that the output power is relatively insensitive to frequency, implying that the device has frequency-tunable characteristics. Since it is proportional to the square of the total current, the output power would increase rapidly with increasing current or with laser power.

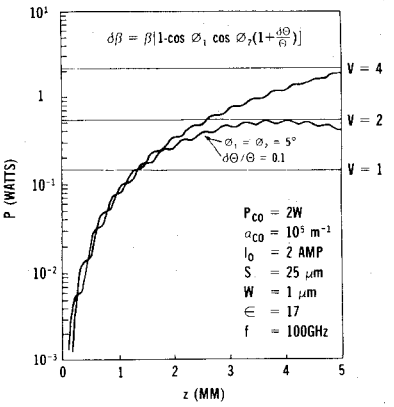

Fig. 5. Millimeter power along the 5-mm long HgCdTe layer in gap of single-ridge guide at 77 K with impedance matched: upper curve is for the phase-match case, while lower curve shows effect of phase mismatch due to laser misalignment.

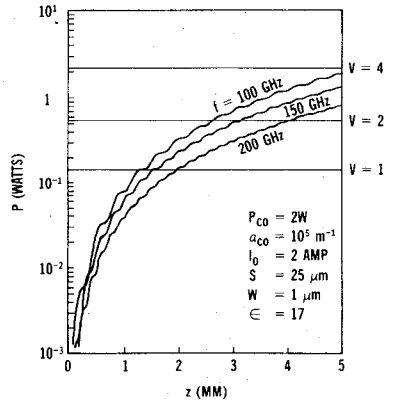

Fig. 6. Millimeter power P along the 5-mm HgCdTe active region in gap of single-ridge guide at 77 K with impedance and phase matched (see Table IV for the other parameter values).

V. CONCLUDING REMARKS

As a solid-state millimeter source, the distributed-source configuration is attractive for at least three reasons. It has high device efficiency, it has high-output power characteristics, and it is potentially compact and lightweight. There are two factors contributing to high device efficiency. First, in the configuration examined in this paper, the laser-induced current which synchronously excites the structure to generate millimeter waves is directly proportional to the laser modulation. With the interference technique, it is theoretically possible to convert 50 percent of the total laser power into the modulation. Second, the current-to-field coupling is inherently strong in the ridge guide structure, because the Schottky-diode modulator, where the millimeter current is induced, occupies the gap region in

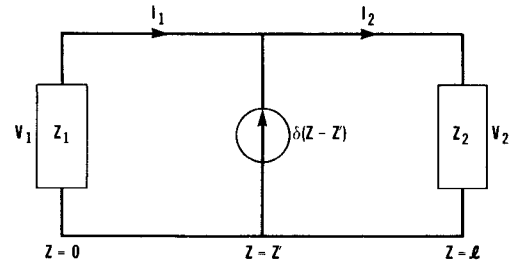

Fig. 7. Diagram of an arbitrarily terminated transmission line.

which the mode fields are concentrated. Perhaps as significant, the calculation indicates that a dielectric-loaded ridge waveguide should provide excellent coupling to other solid-state oscillators. This suggests the examination of, for example, traveling-wave IMPATT's [7] in a ridge-guide configuration. As for the high-power output, analysis and tradeoff study indicate that CW output in the multiwatt range should be realizable providing cooling of the diode material is adequate. Thus far we have only investigated the diode material HgCdTe in some detail. Other materials (for example, InSbAs) may possibly provide better device performance.

Appendix I
Transmission-Line Model

From (10), the transverse voltage V satisfies

$$\frac{d^2V}{dz^2}-ZYV=-ZJ'e^{-\imath\beta' z}, \qquad z_1\leqslant z\leqslant z_2. \tag{A1}$$

We will solve (A1) using the Green's function technique by first finding the voltage response $G(z, z')$ to a point current source at z' on an arbitrarily terminated line. Referring to Fig. 7, $G(z, z')$ satisfies

$$\frac{d^2G}{dz^2}-ZYG=-Z\delta(z-z') \tag{A2}$$

where the delta function $\delta(z-z')$ denotes the unit point current source at $z=z'$. In the figure, Z_0 is the characteristic impedance of the line; Z_1 and Z_2 are the terminating impedances at $z=0$, and $z=l$, respectively; V_i and I_i, $i=1$ or 2, are the voltages and currents. The voltage V due to the traveling current is

$$V(z)=\int_0^l G(z, z')J'e^{-\imath\beta''}dz'. \tag{A3}$$

For notation convenience we define

$$G(z, z')=\begin{cases} V_1(z, z'), & \text{for } 0\leqslant z\leqslant z' \\ V_2(z, z'), & \text{for } z'\leqslant z\leqslant l. \end{cases}$$

The solution of (A2) for $0<z<z'$ is simply

$$V_1=V_{11}e^{\gamma z}+V_{12}e^{-\gamma z} \tag{A4}$$

where $\gamma=\sqrt{ZY}$. Physically, $V_{11}e^{\gamma z}$ is the left-going voltage wave while $V_{12}e^{-\gamma z}$ is the right-going voltage wave in the region $0<z<z'$. The corresponding current I_1 is

$$I_1=-\frac{V_{11}\gamma}{Z}e^{\gamma z}+\frac{V_{12}\gamma}{Z}e^{-\gamma z}. \tag{A5}$$

The voltage-reflection coefficient, ρ_1, at $z=0$ is

$$\rho_1=\frac{Z_1-Z_0}{Z_1+Z_0}. \tag{A6}$$

Equations (A4) and (A5) now simplify to

$$V_1=V_{11}e^{+\gamma z}\left(1+\rho_1e^{-2\gamma z}\right), \qquad 0\leqslant z<z'$$

$$I_1=\frac{V_{11}}{Z_0}e^{+\gamma z}\left(\rho_1e^{-2\gamma z}-1\right), \qquad 0<z<z' \tag{A7}$$

where V_{11} will be determined from the source conditions at $z=z'$. In a similar fashion, the voltage V_2 for $z'<z<l$ is

$$V_2=V_{21}e^{\gamma z}+V_{22}e^{-\gamma z} \tag{A8}$$

and the current I_2 is

$$I_2=-\frac{V_{21}\gamma}{Z}e^{\gamma z}+\frac{V_{22}\gamma}{Z}e^{-\gamma z} \tag{A9}$$

where $V_{21}e^{\gamma z}$ and $V_{22}e^{-\gamma z}$ are the left-going and right-going voltage waves, respectively. Since the voltage reflection coefficient ρ_2 at $z=l$ is

$$\rho_2=\frac{V_{21}}{V_{22}}e^{2\gamma l}$$

(A8) and (A9) simplify to

$$V_2=V_{22}e^{-\gamma z}\left(1+\rho_2e^{2\gamma(z-l)}\right), \qquad z'<z\leqslant l$$

$$I_2=\frac{V_{22}}{Z_0}e^{-\gamma z}\left(1-\rho_2e^{2\gamma(z-l)}\right), \qquad z'<z<l. \tag{A10}$$

At $z=z'$, the voltage must be continuous. This implies that $V_2(z')-V_1(z')=0$; therefore,

$$e^{-\gamma z'}\left(1+\rho_2e^{2\gamma(z'-l)}\right)V_{22}-e^{\gamma z'}\left(1+\rho_1e^{-2\gamma z'}\right)V_{11}=0. \tag{A11}$$

Similarly, the unit current at z' must be equal to $I_2(z')-I_1(z')$; therefore,

$$e^{-\gamma z'}\left(1-\rho_2e^{2\gamma(z'-l)}\right)V_{22}-e^{\gamma z'}\left(\rho_1e^{-2\gamma z'}-1\right)V_{11}=Z_0. \tag{A12}$$

Using Cramer's determinant rule, we have

$$V_{22}=\frac{Z_0e^{\gamma z'}\left(1+\rho_1e^{-2\gamma z'}\right)}{2\left(1-\rho_1\rho_2e^{-2\gamma l}\right)}$$

$$V_{11}=\frac{Z_0e^{-\gamma z'}\left(1+\rho_2e^{2\gamma(z'-l)}\right)}{2\left(1-\rho_1\rho_2e^{-2\gamma l}\right)}. \tag{A13}$$

Substituting the above into the equations for V_1 and V_2, we have the Green's function for an arbitrarily terminated transmission line excited by a point current source at z'

$$G(z_1z')=\begin{cases} \dfrac{Z_0\left(1+\rho_1e^{-2\gamma z'}\right)}{2\left(1-\rho_1\rho_2e^{-2\gamma l}\right)}\left[e^{-\gamma(z-z')}\right. \\ \left.+\rho_2e^{\gamma(z+z'-2l)}\right], \qquad z'\leqslant z\leqslant l \\ \dfrac{Z_0\left(1+\rho_2e^{2\gamma(z'-l)}\right)}{2\left(1-\rho_1\rho_2e^{-2\gamma l}\right)}\left[e^{\gamma(z-z')}\right. \\ \left.+\rho_1e^{-\gamma(z+z')}\right], \qquad 0\leqslant z\leqslant z'. \end{cases} \tag{A14}$$

For our case, where the current source is a traveling wave, extending from $z'=z_1$ to $z'=z_2$, and where the line is impedance matched to $z=0$ and at $z=l$ (see Fig. 7), (A14) reduces to

$$G(z,z')=\begin{cases}\dfrac{Z_0}{2}e^{-\gamma(z-z')}, & z'\leqslant z\\ \dfrac{Z_0}{2}e^{\gamma(z-z')}, & z\leqslant z'.\end{cases} \tag{A15}$$

Using (A3) and (A15) we have

$$V(z)=\frac{Z_0J'}{2}\begin{cases}\dfrac{e^{\gamma z}}{\gamma+i\beta'}\left[e^{-(\gamma+i\beta')z_1}-e^{-(\gamma+i\beta')z_2}\right], & 0\leqslant z\leqslant z_1\\ \dfrac{1}{\gamma-i\beta'}\left(e^{(\gamma-i\beta')z}-e^{(\gamma-i\beta')z_1}\right)+\dfrac{e^{\gamma z}}{\gamma+i\beta'}\left(e^{-(\gamma+i\beta')z_1}-e^{-(\gamma+i\beta')z_2}\right), & z_1\leqslant z\leqslant z_2\\ \dfrac{e^{-\gamma z}}{(\gamma-i\beta')}\left(e^{(\gamma-i\beta')z_2}-e^{(\gamma-i\beta')z_1}\right), & z_2\leqslant z\leqslant l.\end{cases} \tag{A16}$$

Appendix II
Waveguide Model

The differential equation relating the electric field amplitude A to the driving current source J is

$$\frac{d^2A}{dz^2}-\gamma^2A=i\omega\mu\int_{-s/2}^{s/2}J\phi(x)\,dx. \tag{A17}$$

It should be clear that, with some minor modifications, the transmission-line results of Appendix I are applicable here since the two governing differential equations are similar. To see the effect of the waveguide shape and dimensions, however, we will derive the Green's function for (A17) independently of the transmission-line results.

The Green's function $G(z,z')$ satisfies

$$\frac{d^2G}{dz^2}-\gamma^2G=-\delta(z-z') \tag{A18}$$

and the excited field amplitude due to an arbitrary $J(z)$ is then given by

$$A(z)=K\int_{z_1}^{z_2}J(z')G(z,z')\,dz' \tag{A19}$$

where $K\equiv i\omega\mu\int_{-s/2}^{s/2}\phi(x)\,dx$ and $z_1<z<z_2$ is the extent of the current source $J(z)$. Referring to Fig. 7 and following the procedures of Appendix I, we define

$$G(z,z')=\begin{cases}A_1(z,z'), & \text{for } 0\leqslant z\leqslant z'\\ A_2(z,z'), & \text{for } z'\leqslant z\leqslant l.\end{cases} \tag{A20}$$

The solution of (A19) for $0<z<z'$ is

$$A_1=A_{11}e^{\gamma z}+A_{12}e^{-\gamma z} \tag{A21}$$

where $A_{11}e^{\gamma z}$ and $A_{12}e^{-\gamma z}$ are the left and right propagating electric field amplitudes, respectively. From $\boldsymbol{E}=A(z)\phi(x)\hat{y}$ and the Maxwell equation

$$H_x=\frac{\partial A}{\partial z}\frac{\phi(x)}{i\omega\mu} \tag{A22}$$

we obtain

$$H_x=\frac{A_{11}}{i\omega\mu}\left(e^{\gamma z}-\rho_1e^{-\gamma z}\right)\phi(x) \tag{A23}$$

where $\rho_1=A_{12}/A_{11}$ is the amplitude reflection coefficient at $z=0$ given by

$$\rho_1=\frac{Z_1-Z_0}{Z_1+Z_0}. \tag{A24}$$

The field expressions in the region $0<z<z'$ are then

$$E_y=A_1\phi=A_{11}e^{\gamma z}\left(1+\rho_1e^{-2\gamma z}\right)\phi(x)$$
$$H_x=\frac{1}{i\omega\mu}\frac{\partial A}{\partial z}\phi=\frac{A_{11}}{Z_0}e^{\gamma z}\left(1-\rho_1e^{-2\gamma z}\right)\phi(x) \tag{A25}$$

with $Z_0\equiv i\omega\mu/\gamma$ and A_{11} to be determined from the source conditions at $z=z'$.

Similarly, the field amplitude for $z'<z<l$ is

$$A_2=A_{22}\left(e^{-\gamma z}+\rho_2e^{\gamma z}e^{-2\gamma l}\right) \tag{A26}$$

$$H_x=-\frac{A_{22}}{Z_0}\left(e^{-\gamma z}-\rho_2e^{\gamma z}e^{-2\gamma l}\right)\phi(x) \tag{A27}$$

where $\rho_2=V_{21}/V_{22}e^{2\gamma l}$ is the reflection coefficient at $z=l$. The field expressions for $z'\leqslant z\leqslant l$ are then given by

$$E_y=A_2\phi(x)=A_{22}e^{-\gamma z}\left(1+\rho_2e^{\gamma z(z-l)}\right)\phi(x)$$
$$H_x=\frac{\partial A_2}{\partial z}\frac{\phi(x)}{iw\mu}=-\frac{A_{22}}{Z_0}e^{-\gamma z}\left(1-\rho_2e^{2\gamma(z-l)}\right)\phi(x). \tag{A28}$$

At $z=z'$, E_y must be continuous and so

$$e^{-\gamma z'}\left(1+\rho_2e^{2\gamma(z'-l)}\right)A_{22}=e^{\gamma z'}\left(1+\rho_1e^{-2\gamma z'}\right)A_{11}. \tag{A29}$$

Now the magnetic field H_x at z' must be discontinuous to account for the point current source there. Quantitatively, from (A18), we have

$$\frac{d}{dz}A_2(z')-\frac{d}{dz}A_1(z')=-1 \tag{A30}$$

and so,

$$e^{-\gamma z'}\left(1-\rho_2e^{2\gamma(z'-l)}\right)A_{22}+e^{\gamma z'}\left(1-\rho_1e^{-2\gamma z'}\right)A_{11}=Z_0. \tag{A31}$$

Since these equations are similar to those for the transmission-line case in Appendix I, the procedures for finding the Green's function are identical and, therefore, will not be repeated here.

Appendix III
Wave-Vector Error Due to Misalignment Errors

Let z be the true direction of propagation along the waveguide axis for the perfect phase-match case, and z' be the perturbed direction. We see from Fig. 8 that the alignment between the two lasers is described by the angle

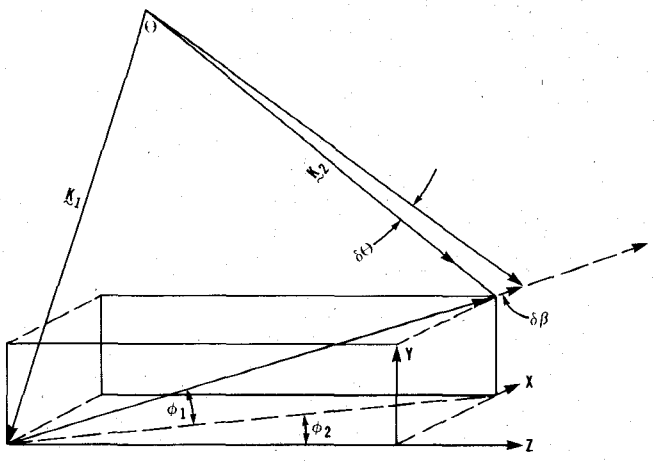

Fig. 8. Diagram of wave-vector mismatch due to laser misalignment.

θ, and that the laser misalignment with respect to the z axis (waveguide axis) is described by ϕ_1 and ϕ_2. Let $\beta\hat{z}$ be the wave vector of the dominant mode to be phase matched by the induced current source. Ideally, we would like to have

$$\boldsymbol{k}_1-\boldsymbol{k}_2=\beta\hat{z}. \tag{A32}$$

Since $|\boldsymbol{k}_1|\simeq|\boldsymbol{k}_2|\equiv k$ for the frequency considered, we have

$$|\boldsymbol{k}_1-\boldsymbol{k}_2|=2k\sin\theta/2. \tag{A33}$$

We see from (A32) and (A33) that the conditions for perfect phase match are

$$2k\sin\theta/2=\beta \tag{A34}$$

$$\frac{\boldsymbol{k}_1-\boldsymbol{k}_2}{|\boldsymbol{k}_1-\boldsymbol{k}_2|}=\hat{z}.$$

For angle error $\delta\theta\ll\theta$

$$|\boldsymbol{k}_1-\boldsymbol{k}_2|=2k\sin\frac{\theta}{2}+k\cos\frac{\theta}{2}\delta\theta=\beta+\delta\beta \tag{A35}$$

and the corresponding z component β' is then given by

$$\beta'=\left[2k\sin\frac{\theta}{2}+k\cos\left(\frac{\theta}{2}\right)\delta\theta\right]\cos\phi_1\cos\phi_2. \tag{A36}$$

The overall wave-vector mismatch ($\delta\beta$) resulting from the misalignment angle $\delta\theta$, and the orientation angles ϕ_1 and ϕ_2, is then given by

$$\delta\beta=\beta-\beta'=\beta\left(1-\cos\phi_2\cos\phi_1\left(1+\frac{\delta\theta}{\theta}\right)\right). \tag{A37}$$

REFERENCES

[1] S. M. Sze, *Physics of Semiconductor Devices*. New York: Wiley, 1977, ch. 5.

[2] S. M. Sze and R. M. Ryder, "Microwave avalanche diodes," *Proc. IEEE*, vol. 59, pp. 1140–1154, Aug. 1971.

[3] P. J. Meier, "Integrated fin-line millimeter components," *IEEE Trans. Microwave Theory Tech.*, vol. MTT-22, pp. 1209–1216, Dec. 1974.

[4] S. Hopfer, "The design of ridged waveguide," *IEEE Trans. Microwave Theory Tech.*, vol. MTT-3, pp. 20–29, Oct. 1955.

[5] W. J. Gettsinger, "Ridge waveguide field description and application to directional couplers," *IEEE Trans. Microwave Theory Tech.*, vol. MTT-10, pp. 41–50, Jan. 1962.

[6] S. B. Cohn, "Properties of ridge waveguide," *Proc. IRE*, vol. 35, pp. 783–788, Aug. 1947.

[7] M. Franz and J. B. Beyer, "The traveling-wave IMPATT mode," *IEEE Trans. Microwave Theory Tech.*, vol. MTT-26, pp. 861–865, Nov. 1978.

Jack SooHoo received the B.S. and M.S. degrees from the University of California at Berkeley in 1960 and 1962, respectively, and the Ph.D. degree from Stanford University, Stanford, CA, in 1971, all in electrical engineering.

He was with Lockheed Palo Alto Research Laboratories from 1961 to 1966, and was a Lockheed Coop Student and Research Assistant at Stanford from 1966 to 1971, working in the areas of electromagnetics, acoustics, and nonlinear optics. He has been with Rockwell International since 1971, currently doing work in electrooptic, laser, and millimeter-wave technologies. He is also a Lecturer in the Department of Electrical Engineering at the University of California, Irvine.

✤

Shi-Kay Yao (S'68–M'74–SM'80) was born in China on June 30, 1945. He received the B.S. degree in electrical engineering from National Taiwan University, Taipei, Republic of China, in 1967, and the M.S. and Ph.D. degrees in electrical engineering from Carnegie-Mellon University, Pittsburgh, PA, in 1969 and 1974, respectively.

He is currently Senior Scientist at the TRW Technology Research Center, Torrance, CA, contributing to the development of optoelectronic devices and fiber optical communication. Prior to this, he was Manager of Optical Signal Processing at the Electronics Research Center of Rockwell International, Anaheim, CA, from 1976 to 1980, where his major contributions were in integrated optics, waveguide optical lenses, waveguide photodetectors, and surface acoustooptic devices using ZnO piezoelectric thin film. He was with Harris Corporation from 1974 to 1976 working on acoustooptic devices and surface acoustic wave devices. He has been working on optical image processing (1968–1970), laser communication (1970–1973) as part of his Ph.D. dissertation requirement, and integrated optical switching devices on $LiNbO_3$ (1973–1974) as post doctorate research, at Carnegie-Mellon University. He is the author or coauthor of over 40 journal articles, technical presentations and holds several U.S. patents.

Dr. Yao is currently the Treasurer of the Los Angeles chapter of IEEE Quantum Electronics and Applications Society. He is a member of the Optical Society of America, Eta Kappa Nu, and Sigma Xi.

✤

James E. Miller was born in Saint Louis, MO, in 1943. He received the B.S. degree in physics and the B.A. degree in mathematics in 1964 and the M.S. degree in physics in 1966 from Texas A & M University, College Station.

He worked for Texas Instruments, Dallas, TX, from 1966 to 1968 primarily on nondestructive characterizing of silicon epitaxial layers. In 1968 he joined the staff of the U.S. Army Night Vision & Electro-Optics Laboratory, Fort Belvoir, VA. His areas of work have been optically pumped laser material development and injection laser growth and fabrication. Currently, he is engaged in millimeter wave detector and source research.

✤

Richard R. Shurtz, II, was born in Athens, OH. on December 20, 1946. He received the B.S. degree in physics from the University of Arkansas, Fayetteville, in 1968 and the M.S. and Ph.D. degrees in physics from The Catholic University, Washington, DC, in 1971 and 1975, respectively.

In 1968 he joined the staff of the Night Vision and Electro-Optics Laboratory, Fort Belvoir, VA, and has worked on injection lasers, IR sensor physics, and millimeter wave sources and detectors. He is currently Team Chief of the Near Millimeter Wave Team.

Yuan Taur was born in Kiangsi, China, on September 27, 1946. He received the B.S. degree from National Taiwan University, Taipei, Taiwan, in 1967, and the Ph.D. degree in physics from the University of California, Berkeley, in 1974.

During 1975–1979, he worked at NASA Goddard Institute for Space Studies, New York, on low-noise Josephson-junction mixers at millimeter wavelength. Presently he is with Rockwell International Science Center, Thousand Oaks, CA. His current research activity is in solid-state infrared/millimeter-wave sources and detectors.

✤

R. A. Gudmunsen (M'55–SM'57), photograph and biography not available at time of publication.

A Method for Diminishing Total Transmission Losses in Curved Dielectric Optical Waveguides

MASAHIRO GESHIRO, MEMBER, IEEE, AND SHINNOSUKE SAWA, MEMBER, IEEE

Abstract—**A practical method for diminishing total transmission losses in curved dielectric optical slab waveguides is proposed. Asymmetric structures are introduced into curved sections. It is found that there exists an optimum asymmetric structure for the curved section which makes the total transmission loss minimum. And it is also found that the characteristics of total transmission loss do not critically depend upon the asymmetry of waveguide structure, so that some displacement from the optimum structure does not increase the loss in an appreciable amount.**

I. Introduction

PROPAGATING modes along a circular bend of dielectric waveguide suffer from a pure bending loss which mainly depends upon waveguide structure and curvature radius. In addition, a transition loss due to transformed radiation modes is incurred as soon as a propagating mode passes through a junction where two waveguides of different curvature radii are connected. Up to date, these two types of losses in several kinds of dielectric waveguides have been analyzed in detail separately [1]–[5]. A few reports have treated a total transmission loss which must be evaluated by taking both kinds of losses into consideration [6], [7].

Generally speaking, these losses must be decreased to the smallest possible amount in the application of dielectric waveguides to optical integrated circuits. Therefore, the loss reduction is an important problem which must be solved quickly from the practical point of view. To the authors' knowledge, however, it seems that methods for diminishing the total transmission loss have been scarcely presented.

Taking account of the well-known fact that the characteristics of each kind of loss are strongly affected by the waveguide structure, we can expect the improvement in the total transmission-loss characteristics provided that the waveguide structure is controlled appropriately. In the present paper, a practical method is proposed for diminishing the total transmission loss of a step-index dielectric optical slab waveguide containing a circular bend. An asymmetric index distribution is introduced into a curved section which connects two straight waveguides of symmetric index distribution. Though a very simple and easy method, it has an excellent effect on the total transmission loss as shown in the following sections.

The analysis is based on the assumption that the total transmission loss is given by the sum of pure bending loss and transition loss. This assumption may be good when the curved section is not perturbed and long enough compared with the wavelength of light. The pure bending loss is calculated by using the convenient approximate method presented by Marcuse [2]. The transition loss at the junction is estimated by the overlap integral of the wave functions in both sections. The perturbation solution is used for the wave function of curved section [8].

II. Pure Bending Loss

A curved dielectric optical slab waveguide and a cylindrical coordinate system are shown in Fig. 1. The center of curvature coincides with the z axis of the coordinate sys-

Manuscript received March 16, 1981; revised June 29, 1981.

The authors are with the Department of Electronics Engineering, Faculty of Engineering, Ehime University, 3, Bunkyo-cho, Matsuyama City, Ehiime 790, Japan.

0018-9480/81/1100-1182$00.75 ©1981 IEEE